Letter

Detection and Classification of Non-Photosynthetic Vegetation from PRISMA Hyperspectral Data in Croplands

Monica Pepe [1] , **Loredana Pompilio** [1,]*, **Beniamino Gioli** [2] **and Lorenzo Busetto** [1] **and Mirco Boschetti** [1]

[1] Institute for Electromagnetic Sensing of the Environment, National Research Council of Italy, via Bassini 15, 20133 Milano, Italy; pepe.m@irea.cnr.it (M.P.); busetto.l@irea.cnr.it (L.B.); boschetti.m@irea.cnr.it (M.B.)

[2] Institute of Bioeconomy, National Research Council of Italy, via Madonna del Piano, 10-50019 Sesto Fiorentino, Italy; beniamino.gioli@cnr.it

[*] Correspondence: pompilio.l@irea.cnr.it

check for updates

Abstract: This study introduces a first assessment of the capabilities of PRISMA (PRecursore IperSpettrale della Missione Applicativa)—the new hyperspectral satellite sensor of the Italian Space Agency (ASI)—for Non-Photosynthetic Vegetation (NPV) monitoring, a topic which is becoming very relevant in the field of sustainable agriculture, being an indicator of crop residue (CR) presence in the field. Data-sets collected during the mission validation phase in croplands are used for mapping the NPV presence and for modelling the diagnostic absorption band of cellulose around 2.1 μm with an Exponential Gaussian Optimization approach, in the perspective of the prediction of the abundance of crop residues. Results proved that PRISMA data are suitable for these tasks, and call for further investigation to achieve quantitative estimates of specific biophysical variables, also in the framework of other hyperspectral missions.

Keywords: hyperspectral remote sensing; non-photosynthetic vegetation; PRISMA

1. Introduction

Non-photosynthetic vegetation (NPV) refers to vegetation that cannot perform a photosynthetic function, thus including standing dead vegetation, surface plant litter and crop residues. The presence of NPV on land plays an important role in the cycling of carbon, nutrients and water in both natural and anthropic environments [1,2]. In the framework of sustainable agriculture, the practice of low-intensity tillage and the application of crop residues after harvest on agricultural fields contributes to soil conservation [3], through the interaction of physical, biophysical and chemical processes.

The presence of a layer of dead vegetation on topsoils inhibits moisture evaporation from soil, provides protection against wind and water erosion [4], reduces soil compaction due to agricultural machinery and improves the soil structure. Such practise also allows to increase the nutrients content in soil (organic carbon and nitrogen), control the carbon uptake (including CO_2 fixing), and regulate water flows (infiltration, evaporation, runoff) [5–7]. Keeping crop residues is therefore a fundamental aspect for preserving soil-related agri-ecological conservation functions, based on low-intensity tillage, permanent soil cover and crop rotation.

The accurate identification of NPV to assess crop residue presence at the scale of single parcels is crucial for monitoring and verification actions on the implementation of conservation agriculture, in agreement with the sustainable agriculture pillar of the forthcoming EU Common Agriculture Policy [8]. This task can improve crop and environmental monitoring only if a correct and timely

detection and estimation of crop residue (CR) against bare soil (BS) and green vegetation (GV) cover is achieved [9].

Remote Sensing can provide valuable techniques to assess the presence of NPV over large areas through the analysis of aerial and satellite data [6,10,11]. Hyperspectral Narrow Bands (HNB) data proved to be more efficient and reliable than multispectral broadband (MSBB) data [1,12–14] for two main reasons: (i) hyperspectral sensors allow for the recognition of even subtle absorption features, as those diagnostic of carbon-based constituents (CBC) of Crop Residues, such as cellulose, lignin, hemicellulose and starch [15,16]; (ii) CBCs exhibit diagnostic absorption features mainly in the short-wave infrared (SWIR), a spectral region where most multispectral sensors provide limited information, having few and coarse resolution bands. Since crop residues show many diagnostic features in the range 1.6–2.3 µm to be distinguished from soils [17], high spectral resolution in the SWIR is desirable. In particular, cellulose and lignin exhibit well-known diagnostic absorption features at approximately 2.1 and 2.3 µm [12,15,17].

New opportunities to provide quantitative estimates of NPV may arise from next-generation HNB space data, either from already availble satellite sensors as ASI–PRISMA or planned for launch, as the DLR Environmental Mapping and Analysis Program (EnMAP), or under study, such the NASA Surface Biology and Geology (SBG) observing system and the Copernicus Hyperspectral Imaging Mission (CHIME). In this framework the scientific community is called to address two specific issues: (i) CR detection through classification of HNB data in order to provide tools for monitoring and verification of conservation agricultural practices and (ii) CR quantification through the estimate of biophysical parameters (cellulose and lignine) as indicators of environmental processes.

In order to address these questions we first made an exploratory analysis comparing PRISMA data with in situ spectra to verify the presence of the 2.1 µm feature diagnostic of cellulose, then we processed PRISMA data across a series of field surveys in two Italian regions with two main objectives: (1) NPV detection at the scale of single parcels through object-based classification and (2) spectral characterisation of the 2.1 µm absorption feature in NPV as a first step towards quantitative approaches.

2. Materials and Methods

2.1. PRISMA Satellite Data

PRISMA (PRecursore IperSpettrale della Missione Applicativa) is an hyperspectral satellite system launched on 22 March 2019 by the Italian Space Agency (ASI) on a low-Earth, Sun-synchronous orbit at 615 km altitude. The mission takes advantage of the combination of: (i) two hyperspectral sensors in the spectral range 400–2500 nm (around 240 channels, overlapping between 920 and 1010 nm) with a GSD (Ground Sampling Distance) of 30 m and average spectral resolution less than 10 nm; (ii) a panchromatic camera working in the spectral range 400–700 nm with a GSD of 5 m (Table 1). The mission program is mainly addressed to research entities and government agencies to fulfil the requirements of selected EO applications related to environmental monitoring and protection, and sustainable development [18]. The system is important for the manifold applications requiring HNB data, and as a forerunner (the meaning of Italian *Precursore*) for similar forecoming or in-progress missions.

Figure 1 shows the areas of investigation that correspond to two large farms located in northern Italy (Jolanda di Savoia—JDS, 3800 ha) and in Sardinia (Arborea—ARB, 1000 ha). They show complex agricultural landscapes with different crops and varieties, as reported in the crop maps also shown in Figure 1. Two cloud-free PRISMA scenes were successfully acquired in 2019 at ARB estate (on 24–25 August, hereafter referred as images A1 and A2, respectively), and one at JDS on 14 July 2020 (image J1).

Table 1. Main features of PRISMA hyperspectral mission.

Feature	Description
Orbit altitude reference	615 km
Field of View (FOV)	2.77°
Instantaneous FOV	48 mrad
Swath	30 km
Ground Sampling Distance	Hyperspectral camera: 30 m; Panchromatic camera: 5 m
Spectral range	VNIR: 400–1100 nm (66 bands); SWIR: 920–2500 nm (173 bands)
Signal-to-noise ratio	VNIR: >160 (450 at 650 nm); SWIR: >100 (>360 at 1550 nm); PAN: >240
Spectral Width	≤14 nm
Spectral Calibration Accuracy	±0.1 nm
Radiometric quantization	12 bits
Repeat cycle	29 days (450 orbits)
Relook time	<7 days
Lifetime	5 years
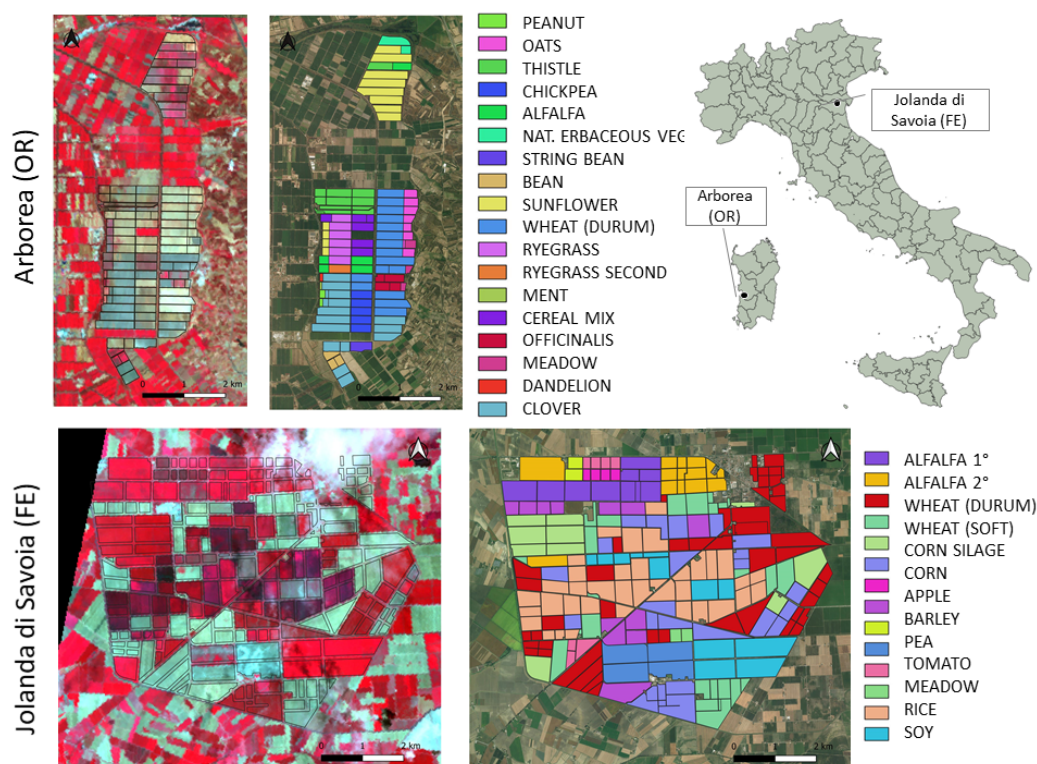
Figure 1. Study areas of the PRISCAV project: their geographic framework, crop maps and false colour composite PRISMA data used in this study.

2.2. PRISCAV Fiducial Reference Measurements

Within the PRISMA mission framework, the project PRISCAV (PRISMA mission cal/val scientific activities) is aimed at evaluating sensor performance, products and processor by the use of Fiducial Reference Measurements (FRM) collected at the same time of satellite overpasses. FRM are spectroradiometric observations of Elementary Sampling Units (ESUs) placed at selected sites. Field measurements procedure has been specifically designed for PRISCAV, according to the protocols of Quality Assurance framework for Earth Observation (QA4EO) endorsed by the Committee on Earth Observation Satellites, and the ESA project FRM4VEG (Fiducial Reference Measurements for Vegetation, originally designed for Sentinel-2, -3, and PROBA-V). This protocol at agricultural sites

consisted in measuring reflectance (obtained as the ratio of the radiance reflected from a Spectralon reference panel and from the target in a hemispherical/conical configuration, according to [19]) over 13 to 17 points distributed as in Figure 2. Measurements were made with a portable Spectral Evolution SM-3500 spectroradiometer operating in the wavelength interval 350–2500 nm, with spectral resolution ranging from 3.5 to 10 nm, equipped with 25° foreoptic. 10 instrument scans per point were acquired with nadiral view at 1.5 m distance from the target surface. Measurements were collected in 2 h time spanning each satellite overpass. Contemporary to PRISMA overpasses, 9 ESUs were measured and archived at ARB test site, while 5 ESUs were collected in the field at JDS.
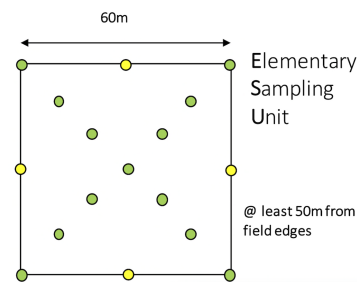

Figure 2. PRISCAV Elementary Sampling Unit setup: each dot is a measurement point (sequence reference panel—target), green dots are the mandatory, while yellow ones are optional.

2.3. Data Processing

The different data sets exploited in this study-field FRM data and PRISMA imagery-with their characteristics and analysis are summarized in Table 2. PRISMA data were downloaded as L1 products (top-of-atmosphere calibrated radiance), then converted to ENVI format and re-projected with a geographic lookup table (GLT) Bowtie Correction through *prismaread*, an R-based open-source software properly developed by [20]. *Prismaread* also extracts ancillary information related to atmospheric correction (band centers and FWHM, Sun and View angles, etc.), which has been performed with ATCOR radiative transfer code (version 9.3.0).

As preliminary analysis, the FRMs of different targets (ESU) were averaged and compared to bottom-of-atmosphere PRISMA spectra in the pixels corresponding to the position of each ESU in the field, to assess the relevance of PRISMA signal between 2.0 and 2.2 µm. Subsequently, reflectance spectra in the selected interval were modelled as uni-variate quadratic functions of the wavelength: $F(\lambda) = a\lambda^2 + b\lambda + c$, where λ is the wavelength. If the absorption is present, *a* coefficient (*Coeff−a* hereafter) is positive, otherwise it is negative.

Table 2. Characteristics of data set and analysis. Meaning of abbreviations: (FRM) in situ spectroradiometric Fiducial Reference Measurements, (SAT) contemporary acquisition of PRISMA data, (FA) Feature Analysis on cellulose absorption band, (DET) mapping category (i.e., NPV), and (CHA) characterisation by application of the Gaussian spectral optimization modelling.

Site/Date	Type	Land Cover	FRM	SAT	FA	DET	CHA
ARB 04 July 2019	VEG	alfalfa	X	-	X	-	-
	NPV	harvested durum wheat	X	-	X	-	X
	SOIL	seedbed (secondary tillage)	X	-	X	-	-
ARB 24–25 August 2019	VEG	alfalfa, bean	X	X	X	-	-
	NPV	harvested wheat, unc. land	X	X	X	X	X
	SOIL	bare soil (primary tillage)	-	X	X	-	-
JDS 14 July 2020	VEG	alfalfa	X	X	X	-	-
	NPV	harvested wheat and barley	X	X	X	X	X
	SOIL	bare soil (primary tillage)	X	X	X	-	-

This approach proved to be effective also for NPV detection on PRISMA imagery (first objective of the study). Based on this algorithm, each parcel has been classified as "*NPV covered*" if the *Coeff−a* was positive, otherwise "*OTHER*". Since the relevant information for monitoring conservation agri-practices is requested at the scale of single parcels, the classification approach was object-based and the known field boundaries were used to extract average spectral signatures per parcel. To avoid border and adjacency effects an internal buffer of 30 m was applied per parcel. Figure 3 shows how the approach works on the mean spectral signatures of three fields presenting different crop conditions in PRISMA J1 image: CR(panel a), BS (panel b) and GV (panel c).
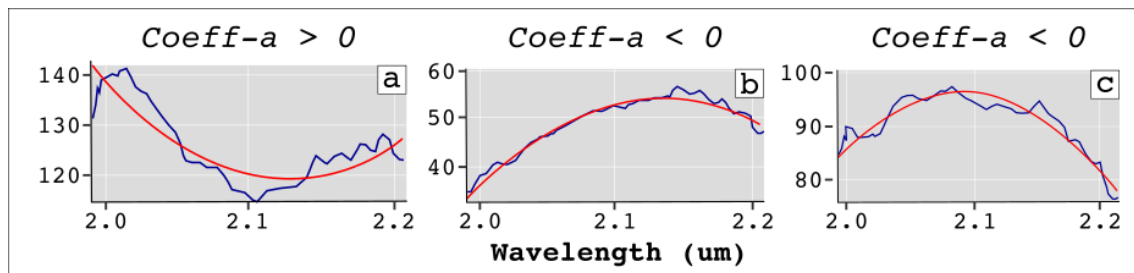
Figure 3. Examples of quadratic fitting of reflectance spectra of (**a**) crop residues CR, (**b**) bare soil BS, and (**c**) green vegetation GV.

To perform spectroscopic characterisation of cellulose absorption band (second objective), the Exponential Gaussian Optimization (EGO) approach [21,22] was applied. For this analysis, we used a dataset composed of PRISMA spectra extracted from 4 parcels of ARB estate in A1 and A2 images, and 3 parcels of JDS estate, in J1 image, where CR conditions were observed at the time of the survey. 15 spectra per parcel were selected and EGO modelling applied in the wavelength interval 2.0–2.2 μm.

EGO models the logarithmic reflectance of absorption features as a function of wavenumbers, as shown in Figure 4b. As part of the exponential Gaussians family, each EGO profile is fully described with its: centre position, width, and depth (as a basic Gaussian function), together with two additional parameters which account for typical non-Gaussian behaviours of absorption bands in the reflectance domain, interpreted as asymmetry or saturation effects. When the EGO extra parameters approximate zero, the absorption band can be modelled as a single Gaussian superimposed on a proper background. Continuum is modelled as a linear function of wavenumber, and thus includes slope and intercept as additional parameters. The analytical EGO routine has been implemented in R, and a Graphical User Interface is also provided for running the optimization, which is based on a Levenberg–Marquardt approach. The goodness of fit (GOF) was evaluated through several metrics, such as the standard error of the estimate (SEE), the coefficient of determination and adjusted coefficient of determination (R^2 and R_{adj}^2, respectively) for multiple regressions, the computation of the Hessian matrix, and the Akaike's Information Criterion (AIC). In this study the target absorption band, as obtained from A1, A2 and J1 images, has been modelled with a basic Gaussian and a linear continuum.
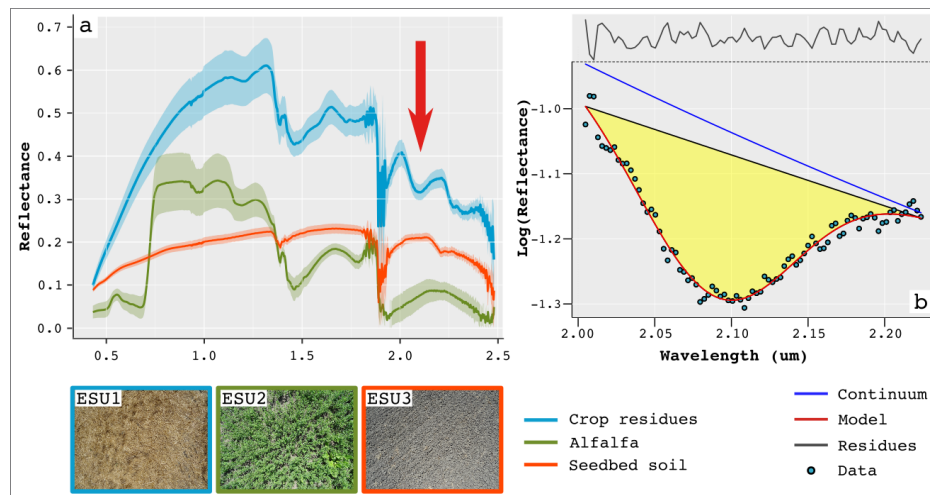
Figure 4. Evidences of absorption feature at 2.1 μm in field spectra collected on July 4th at ARB test site: as shown in panel (**a**) the feature is absent for alfalfa and seedbed soil, while it is present for crop residues. (**b**) The 2.1 μm feature modelled with EGO and results shown.

3. Results

3.1. Exploratory Analyses on Cellulose Absorption Band on PRISMA Data

In order to accomplish the first objective of the present study, the spectra collected in the field at both target sites were analysed to identify spectral features diagnostic of crop residues. One of the features clearly recognized as a candidate for detection of NPVs is the absorption band centered at 2.1 μm [6]. This feature only appears in CR targets, while it is absent in GV and BS targets, as shown in Figure 4a.

Comparison of PRISMA data with in situ measurements on match-ups proved overall a very good agreement on different targets, and this general behaviour is respected also in the band of interest for NPV (Figure 5). Therefore, that particular absorption band has been further investigated to allow NPV detection from PRISMA data and in the perspective of a quantitative analysis of CR.
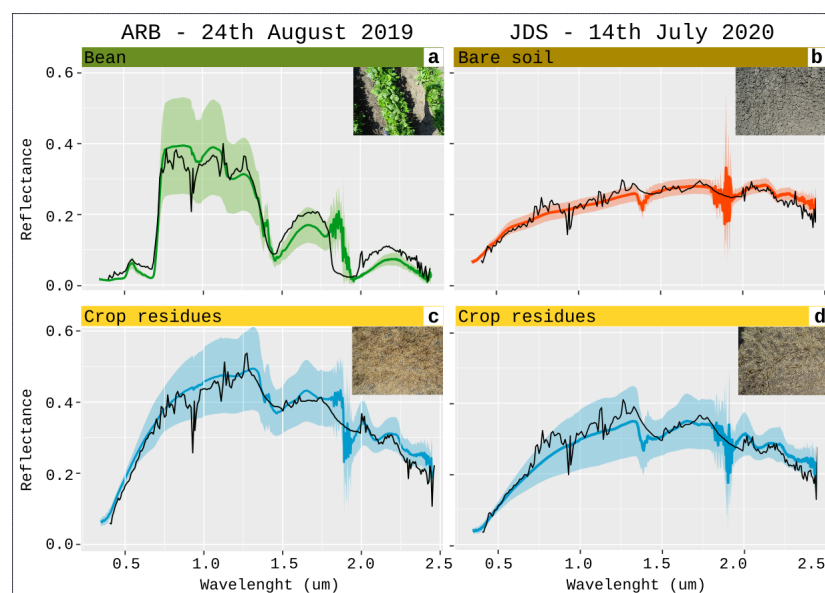

Figure 5. Comparison of PRISMA (A1 image on the left and J1 image on the right) and FRM reflectance spectra acquired on different targets: (**a**) bean, (**b**) bare soil, (**c**,**d**) NPV. Average field measurements are displayed with solid coloured lines, their standard deviations as shaded areas, and PRISMA spectra are in solid black lines.

3.2. NPV Detection at Field Level from Satellite Data

On the base of the spectral behaviour in the 2.0–2.2 µm interval, PRISMA images A1 and J1 have been classified at the scale of parcel, as described in Section 2.3, and the results evaluated by comparison with crop maps, used as reference ground truth. Source images are shown in Figure 1 in CIR composite (R band 52–855 nm, G band 32–650 nm and B band 20–546 nm). Since data were acquired in full summer, fields highlight the condition where winter crops (mainly cereals) present either senescent vegetation, crop residues after harvest or bare soil due to land preparation (i.e., first tillage) for the following crop season.

Figure 6 shows statistics of (*Coeff−a*) for images A1 (left panel) and J1 (right panel). Positive *Coeff−a* values reflecting the presence of cellulose absorption at 2.1 µm are achieved for parcels where winter cereals (*durum wheat*, *soft wheat* and *barley*) were already harvested and CR cover was present in summer, at the moment of PRISMA overpass. The remaining parcels were in vegetative stage or in bare soil conditions, as shown by negative *Coeff−a* values. In image A1 (left panel) also farm areas set aside with natural herbaceous vegetation and ryegrass show positive *Coeff−a* values. Direct observations during field surveys confirmed that these areas actually presented NPV cover: ryegrass was already mowed leaving dry vegetation, while uncultivated parcels showed a majority of senescent vegetation.

Figure 7a shows the results of object-based classification of PRISMA A1 image, according to *Coeff−a* values, as calculated from average PRISMA spectra per parcel. Parcels achieving positive *Coeff−a* are labelled as NPV and shown in red colour, otherwise in blue. Figure 7b shows a false color composite of PRISMA A1 image overlaid with parcel boundaries (black lines). The parcels with *Durum wheat* growings (highlighted in yellow) were already harvested and thus covered with CR. By looking at the *Coeff−a* values computed for those parcels (panel c), four of them show negative values and thus cannot be classified as NPV cover. Nevertheless, those parcels were already ploughed at the time of satellite overpass and therefore were bare soil surfaces, as directly observed during field survey.
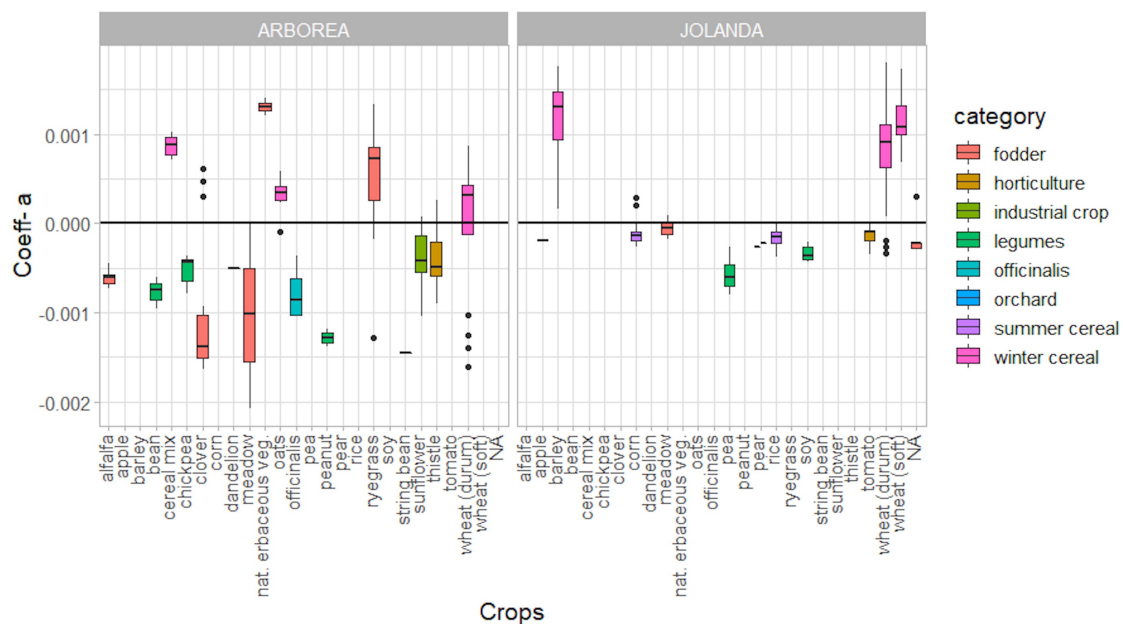

Figure 6. Distribution of *Coeff−a* by crop categories in the two farms. On each target site, boxplots represent the distribution of *Coeff−a* values, as computed on average spectra per parcel and aggregated by crop types. Different colours represent major crop categories.

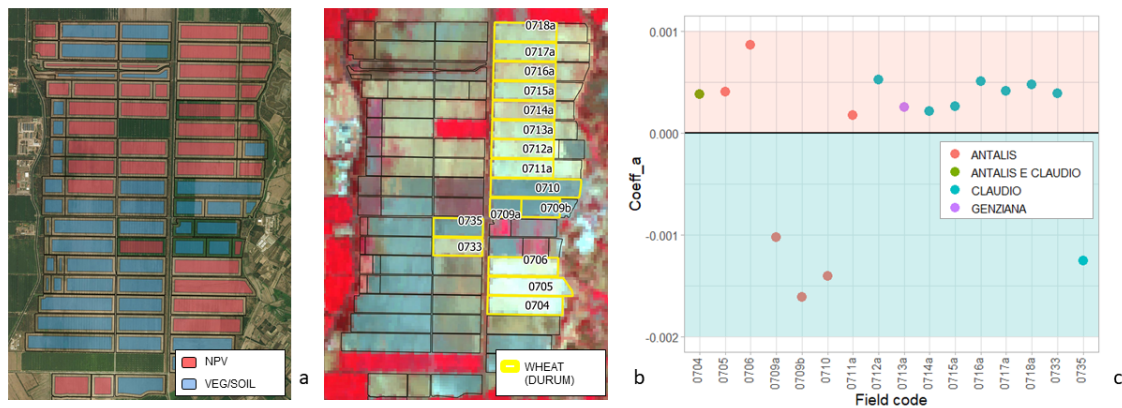**Figure 7.** (**a**) Parcel-based NPV map; (**b**) Pseudocolor CIR composite of PRISMA A1 image, with parcel boundaries of *Durum wheat* growings highlighted in yellow; (**c**) *Coeff−a* values computed by modelling the average spectra per parcel only for *Durum wheat* growings. Parcel IDs are shown in (**b**) and as X-axis in (**c**).

3.3. Spectroscopic Characterisation of Cellulose Band in PRISMA Data

The potential of PRISMA data to provide indicators of NPV presence was evaluated through modelling the cellulose absorption band with the EGO approach, as described in Section 2.3 and shown in Figure 4b.

Figure 8 displays the results of EGO modelling, at both test sites for winter cereal harvested fields (IDs on X-axis). The different species/varieties in the two sites are highlighted with different gray tones background: *Durum wheat* is present in IDs: 704, 705, 706, 711 and 358, *Barley* in ID 331 and *Soft wheat* in ID 45. The results are very consistent and summarized below:

- feature centres are slightly variable within each site, while they are consistent in images A1 and A2. This evidence could be related to the chemical composition of the residues in the two farms or to the influence of the soil background on the spectra, and therefore is worth of further investigation;
- variations of feature widths appear related to the investigated species: the feature is broader for *Barley* and *Soft wheat* with respect to *Durum wheat*, in spectra belonging to both sites;
- as expected, a large variabilty is observed in feature depth, because it is generally related to the abundance of the molecule responsible of the observed spectral feature (cellulose in this case). Thus, feature depth shows to be sensitive to the CR forerunner (*Barley* and *Soft wheat* have deeper bands than *Durum wheat*), and likely to the crop primary productivity (variations within the *Durum wheat* species). In case of *Durum wheat* growings, the lowest feature depth observed in parcel ID711, could be related to the different soil composition of that field which has a higher amount of sand over loam and clay than the other parcels.
- continua slopes vary with species (as for J1 data), while when analysed on the same target in two consecutive days (i.e., *Durum wheat* in A1 and A2) they show a sensitivity to the viewing geometry (A1 and A2 images have been acquired with opposite view angles: −17.6 and +13.5, respectively).
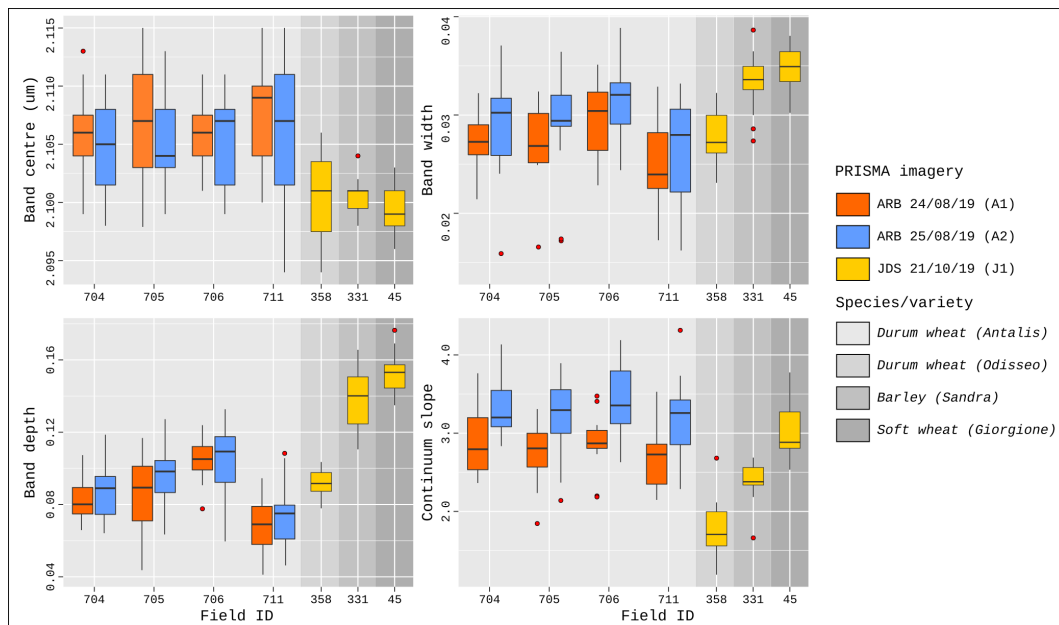
Figure 8. Results of EGO modelling of PRISMA spectra on ARB and JDS test sites. The different panels in clockwise order show the distribution of the EGO parameters: band centre position, band width, continuum slope and band depth; on X-axis are the field IDs; orange, blue and yellow boxes refer to the A1, A2 and J1 images, respectively. Red dots indicate outliers.

4. Discussion

The approaches generally used for NPV detection from optical remote sensing can be grouped into two main types: segmentation of empirical spectral indices, and exploitation of linear spectral unmixing [4,7,9–12]. Both methods have advantages and drawbacks, which have been extensively discussed in [6]. The spectral indices developed so far for NPV estimation in hyperspectral remote sensing are red-edge based or related to the absorption features of cellulose and lignin in the SWIR domain. The latters, which are of interest for the present study, are focused on the computation of band depths, via band ratios or continuum removal techniques [6].

Although functional to the purpose of NPV detection, these approaches use only few channels, and thus do not fully exploit the potential of HNB sensors. The present work demonstrates that (1) the presence of NPV cover can be detected through the modelling of the spectral shape in the 2.0–2.2 μm range of PRISMA data, and (2) the whole informative content of the cellulose diagnostic absorption feature in the SWIR region can be evaluated through EGO modelling.

As shown in Figure 7, the shape of spectra in the wavelength range of interest, when properly modelled, can be used to detect the presence of NPV on ground. In particular, the *Coeff−a* has demonstrated to be a reliable index for object-based classification of single parcels in croplands. The technique of image segmentation used here is based on physical boundaries (which are known from available crop maps in the study areas) and on the assumption that each parcel is a relatively homogeneous region. However, known techniques of object-based image segmentation (as listed in [23]) could be applied in areas where such information is not provided. The main advantages of object-based classification over per-pixel approaches in croplands are the faster computation that reduce time costs and the availability of unique information per parcel, which is the main spatial segmentation unit for implementation of CAP policies [24].

The second point is the retrieval of descriptive parameters of diagnostic features (including the continuum shape) with EGO modelling. As shown in Figure 8, it has the potential to discriminate different covers originating NPVs, to provide information on the soil properties, and to overcome the effects of the viewing geometry.

Indeed the approach adopted here allows to distinguish NPV from bare soil and green vegetation cover at the scale of the single parcel. In the framework of monitoring agronomic practices, further investigations are required to assess spectral differences between senescent vegetation, not yet harvested, and crop residues. Multitemporal approaches can also be used to highligth diagnostic changes of NPV on the same spatial target. Moreover, the influence of soil and weed/vegetation regrowth are aspects to be fully evaluated in order to quantify omission errors of classification, in particular for object-based approaches. More sophisticated machine learning classification techniques will be tested to compare performance and exportability with respect to the physically rule-based one tested here. In our view EGO modelling of absorption region is a way to extract higher level spectroscopic parameters to be used as input variables in machine learning regressive approaches [25]. In order to accomplish quantitative estimates, more extensive field work to qualify absolute crop residue presence and its fractional cover with respect to soil background and vegetation is needed.

5. Conclusions and Perspectives

The analysis presented here is the first attempt to perform the retrieval and the spectral characterization of NPV from PRISMA hyperspectral satellite data, demonstrating their suitability for NPV detection and classification. By modelling the absorption band diagnostic of cellulose in NPVs, we retrieved a number of parameters which fully characterize the spectral feature and potentially can be used to estimate cellulose content for quantitative purposes. Such capabilities are particularly important in the framework of new and forthcoming HNB missions, since PRISMA is the first of a series of hyperspectral satellites that will permit the estimation and prediction of NPV abundance overcoming the limitations of actual MSBB missions in NPV mapping and quantification. Further research should be now directed to developing retrieval methods capable of quantifying cellulose abundance, evaluating the differences among species, and separating the effects of factors such as soil moisture and soil background. The deployment of large scale field experiments, with associated extensive soil and biomass sampling, will permit to build robust linkages between specific biophysical and biochemical variables and spectral features, within inference-based or machine learning frameworks.

Abbreviations

ARB	Arborea
BS	Bare Soil
CBC	Carbon-Based Constituents
CR	Crop Residues
GV	Green Vegetation
JDS	Jolanda di Savoia
HNB	Hyperspectral Narrow Bands
MSBB	Multispectral Broadband
PRISMA	PRecursore IperSpettrale della Missione Applicativa

References

1. Li, Z.; Guo, X. Remote sensing of terrestrial non-photosynthetic vegetation using hyperspectral, multispectral, SAR, and LiDAR data. *Prog. Phys. Geogr.* **2016**, *40*, 276–304. [CrossRef]

2. Hank, T.B.; Berger, K.; Bach, H.; Clevers, J.G.P.W.; Gitelson, A.; Zarco-Tejada, P.; Mauser, W. Spaceborne Imaging Spectroscopy for Sustainable Agriculture: Contributions and Challenges. *Surv. Geophys.* **2019**, *40*, 515–551. [CrossRef]

3. Azzari, G.; Grassini, P., Edreira, J.I.R.; Conley, S.; Mourtzinis, S.; Lobell, D.B. Satellite mapping of tillage practices in the North Central US region from 2005 to 2016. *Remote Sens. Environ.* **2019**, *221*, 417–729. [CrossRef]

4. Arsenault, E.; Bonn, F. Evaluation of soil erosion protective cover by crop residues using vegetation indices and spectral mixture analysis of multispectral and hyperspectral data. *Catena* **2005**, *62*, 157–172. [CrossRef]

5. Kertész, A.; Madarasz, B. Conservation agriculture in Europe. *Int. Soil Water Conserv. Res.* **2014**, *2*, 91–96. [CrossRef]

6. Li, Z. Quantifying Grassland Non-Photosynthetic Vegetation Biomass Using Remote Sensing Data. Ph.D. Thesis, University of Saskatchewan, Saskatoon, SK, Canada, 2017.

7. Hively, W.D.; Lamb, B.T.; Daughtry, C.S.T.; Shermeyer, J.; McCarty, G.W.; Quemada, M. Mapping Crop Residue and Tillage Intensity Using WorldView-3 Satellite Shortwave Infrared Residue Indices. *Remote Sens.* **2018**, *10*, 1657. [CrossRef]

8. E.C. Directorate-General for Agriculture and Rural Development. Modernising and simplifying the CAP—Challenges for agriculture and rural areas: Environment and climate dimensions. In *Agriculture and Rural Development Background Documents*; EC: Bruxelles, Belgium, 2018.

9. Yue, J.; Tian, Q. Estimating fractional cover of crop, crop residue, and soil in cropland using broadband remote sensing data and machine learning. *Int. J. Appl. Earth Obs. Geoinf.* **2020**, *89*, 102089. [CrossRef]

10. Roberts, D.A.; Smith, M.O.; Adams, J.B. Green vegetation, nonphotosynthetic vegetation and soils in AVIRIS data. *Remote Sens. Environ.* **1993**, *44*, 255–269. [CrossRef]

11. Zheng, B.; Campbell, J.B.; de Beurs, K.M. Remote sensing of crop residue cover using multi-temporal Landsat imagery. *Remote Sens. Environ.* **2012**, *117*, 177–183. [CrossRef]

12. Bannari, A.; Staenz, K.; Champagne, C.; Khurshid, K.S. Spatial variability mapping of crop residue using Hyperion (EO-1) hyperspectral data. *Remote Sens.* **2015**, *7*, 8107–8127. [CrossRef]

13. Daughtry, C.S.T.; Graham, M.W.; Stern, A.J.; Quemada, M.; Hively, W.D.; Russ, A.L. Landsat-8 and Worldview-3 Data for Assessing Crop Residue Cover. In Proceedings of IGARSS 2018, Valencia, Spain, 22–27 July 2018; pp. 3852–3855.

14. Dennison, P.E.; Qi, Y.; Meerdink, S.K.; Kokaly, R.F.; Thompson, D.R.; Daughtry, C.S.T; Quemada, M.; Roberts, D.A.; Gader, P.D.; Wetherley, E.B.; et al. Comparison of methods for modeling fractional cover using simulated satellite hyperspectral imager spectra. *Remote Sens.* **2019**, *11*, 2072. [CrossRef]

15. Fourty, T.; Baret, F.; Jacquemoud, S.; Schmuck, G.; Verdebout, J. Leaf optical properties with explicit description of its biochemical composition: Direct and inverse problems. *Remote Sens. Environ.* **1996**, *56*, 104–117. [CrossRef]

16. Berger, K.; Verrelst, J.; Féret, J.B.; Wang, Z.; Wocher, M.; Strathmann, M.; Danner, M.; Mauser, W.; Hank, T. Crop nitrogen monitoring: Recent progress and principal developments in the context of imaging spectroscopy missions. *Remote Sens. Environ.* **2020**, *242*, 111758. [CrossRef]

17. Wang, Z.; Skidmore, A.K.; Wang, T.; Darvishzadeh, R.; Hearne, J. Applicability of the PROSPECT model for estimating protein and cellulose+ lignin in fresh leaves. *Remote Sens. Environ.* **2015**, *168*, 205–218. [CrossRef]

18. Lopinto, E.; Ananasso, C. The Prisma hyperspectral mission. In *Towards Horizon 2020: Earth Observation and Social Perspectives, Proceedings of the 33rd EARSeL Symposium, Matera, Italy, 3–7 June 2013*; Lasaponara R., Masini N., Biscione M., Eds.; EARSeL: Münster, Germany, 2013.

19. Schaepman-Strub, G.; Schaepman, M.E.; Painter, T.H.; Dangel, S.; Martonchik, J.V. Reflectance quantities in optical remote sensing—definitions and case studies. *Remote Sens. Environ.* **2006**, *103*, 27–42. [CrossRef]

20. Busetto, L.; Ranghetti, L. Prismaread: A Tool for Facilitating Access and Analysis of PRISMA L1/L2 Hyperspectral Imagery v1.0.0. Available online: https://lbusett.github.io/prismaread/ (accessed on 4 November 2020).

21. Pompilio, L.; Pedrazzi, G.; Sgavetti, M.; Cloutis, E.A.; Craig, M.A.; Roush, T.L. Exponential Gaussian approach for spectral modeling: The EGO algorithm I. Band saturation. *Icarus* **2009**, *201*, 781–794. [CrossRef]

22. Pompilio, L.; Pedrazzi, G.; Cloutis, E.A.; Craig, M.A.; Roush, T.L. Exponential Gaussian approach for spectral modelling: The EGO algorithm II. Band asymmetry. *Icarus* **2010**, *208*, 811–823. [CrossRef]

23. Najafi, P.; navid, H.; Feizizadeh, B.; Eskandari, I; Blaschke, T. Fuzzy Object-Based Image Analysis Methods Using Sentinel-2A and Landsat-8 Data to Map and Characterize Soil Surface Residue. *Remote Sens.* **2019**, *11*, 2583. [CrossRef]

24. Agricultural Monitoring. Available online: https://ec.europa.eu/jrc/en/research-topic/agricultural-monitoring (accessed on 4 November 2020).

25. Rivera Caicedo, J.P.; Verrelst, J.; Munoz-Marì, J.; Moreno, J.; Camps-Valls, G. Toward a Semiautomatic Machine Learning Retrieval of Biophysical Parameters. *Sel. Top. Appl. Earth Obs. Remote Sens.* **2014**, *7*, 1249–1259. [CrossRef]

Publisher's Note: MDPI stays neutral with regard to jurisdictional claims in published maps and institutional affiliations.